PCCP

Accepted Manuscript




ROYAL SOCIETY OF CHEMISTRY

www.rsc.org/pccp

PCCP
RSCPublishing

COMMUNICATION

# Insight into the Mechanism of Nanodiamond Catalysed Decomposition of Methane Molecules

Cite this: DOI: 10.1039/x0xx00000x

Bingwei Zhong,[a,b] Jian Zhang,*[c] Bo Li,[b] Bingsen Zhang,[b] Chunli Dai,[b] Xiaoyan Sun,[b] Rui Wang[b] and Dang Sheng Su*[b]

Received 00th January 2012,
Accepted 00th January 2012

DOI: 10.1039/x0xx00000x

www.rsc.org/

**Nanodiamond can catalyze the decomposition of methane, and its initial rate is linearly dependent on the number of -CH=CH- defective sites. Thermal treatment improves the ordering of surface atoms, resulting in an inferior activity but a more stable performance over a long period of time, and above 1300°C few-layered graphene can be found.**

Methane as the most inert hydrocarbon has been extremely difficult to activate. Catalytic methane decomposition (CMD) is considered to be one of the most promising routes to produce $CO_x$-free hydrogen,[1] since the carbon atoms are completely transformed into a carbonaceous solid as a useful nanomaterial. Although the energy to crack $CH_4$ molecule is favorable ($\Delta H^{\square}_{298}$=74.8 kJ mol$^{-1}$), CMD process is always conducted at temperatures as high as 700~1100°C due to the strong C-H bonding in the $CH_4$ molecule. A few reports have found that carbon can efficiently catalyze the decomposition of $CH_4$. Compared with Fe, Co, Ni and other transition metals,[2,3] carbon exhibits many advantages such as low cost, more availability, being free of catalyst regeneration, stability against deactivation and simple process. Structural and surface properties of carbon were found to determine its catalytic performance,[4] but no definite conclusion has yet been made on the reaction mechanism for this metal-free process. Carbon nanomaterials featuring controllable surface properties and a variety of chemically active heteroatoms have been widely investigated as the promising candidate to the traditional metal-based catalysts.[5] However, the metal-free carbon catalysis has been limited to only a few reactions like dehydrogenation, selective oxidation, hydrogenation and electrochemical processes.[6] A variety of carbon materials have been investigated as CMD catalysts,[7] but nanodiamond (ND) as a member of carbon allotropes has not been tested over the past few years.

Nanodiamond particles have been considerably studied in the fields of abrasive materials, nanosensors, drug delivery, electron field emission, catalysis and so on. As the particle size approaches 5~8 nm, ND possesses a high surface reactivity for its large number of unsatisfied surface atoms and a large surface/volume ratio. Furthermore, the transition from $sp^3$ to $sp^2$ hybridization state inevitably occurs over the crystal surface to form onion-like carbon (OLC) structure, which can be promoted by annealing at high temperatures.[8] In this article, the commercial ND powder was produced by detonation method at ultrahigh pressure and temperature, then purified by oxidative acids to remove the residual metal particles. The surface is always highly defective and can host a certain amount of functional groups, enduring ND with chemical activity for reactions such as dehydrogenation, transformation, CO oxidation and electrochemical oxidation.[8a,9] Importantly, because the $sp^3$-hybridized carbon atoms tend to graphitize to reduce the energy, the thickness of graphitic shell and the number of surface defects can be well controlled by thermal treatment at elevated temperatures. We focus on the origin of activity for $CH_4$ decomposition by ND and perform detailed characterization of the catalysts to clarify the structure of active sites. To our knowledge, this is the first time to employ ND as catalyst for $CH_4$ decomposition and provide a mechanistic view of this metal-free process.

Figure 1a compares the catalytic activities of different kinds of carbon catalysts for CMD at 850°C. At this temperature (and at 900°C too), blank experiments without catalyst show the conversion of $CH_4$ approaching almost zero. $H_2$ as the prevailing gaseous product gives a hydrogen balance of 100±2%. Purified nanodiamond (ND-f) displayed a superior catalytic performance to other carbons including activated carbon (AC), single-walled nanotubes (SWNT) and multi-walled nanotubes (MWNT). The $CH_4$ conversion on ND-f at the initial period of reaction time is as high as 24.4%, being

around 1.4~5.4 times that on other samples. Even when the conversion decreased to 8.6% after the reaction for 8 hours, ND-f still provided the highest value of $CH_4$ conversion. Actually, the degree of deactivation can be efficiently improved by calcination of ND-f at elevated temperatures. Figure 1b illustrates the time-on-stream profiles of ND-f and calcined ND samples (containing the OLC structure) at 850°C, showing that the initial reaction rate decreased but the stability increased with the calcination temperature. Furthermore, the long-time test for three ND samples in Fig. 1c proved this point evidently. The calcination of ND-f sample at 1300 or 2000°C renders a low initial conversion rate, but a relatively longer life time of the catalyst. Moreover, it was supposed that the deposited carbon during the initial several hours could promote the $CH_4$ conversion rate, but eventually result in the deactivation of catalyst.

The performance of one catalyst is usually determined by its textural and surface properties. Figure 1d illustrates the effects of surface area and surface oxygen content (surface O%) on the initial reaction rate. High surface area normally benefits the catalytic turnover, but, in our case, the initial rate sharply decreased with the BET surface area. It is obviously indicated that the pore structure is not pivotal for this catalytic process. Surface oxygenated groups are usually considered to stimulate the metal-free reactions,[6a,10] while the attempt to correlate the initial rate with surface content of each oxygen component failed. The activity increased over 8 times as the surface O% varied from 0.76% to 2.1%, but raised only a few when O% approached 10.1%.

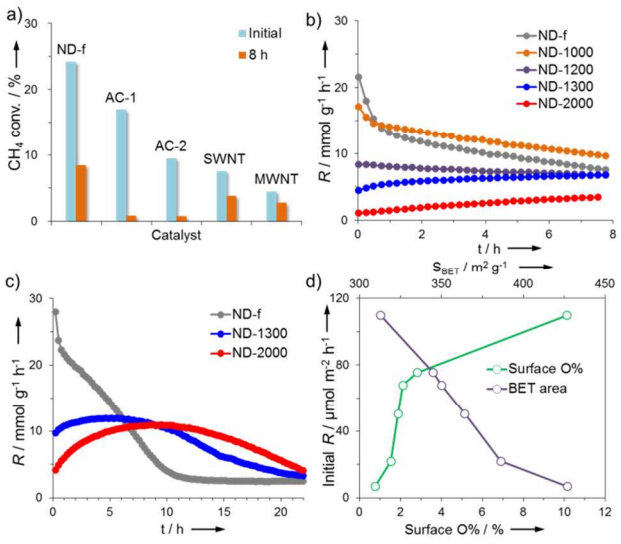


**Fig. 1** a) $CH_4$ conversion of ND-f, AC-1, AC-2, SWNT and MWNT at 850°C. b) Time-on-stream profiles of reaction rate of ND-f and calcined ND samples at 850°C. c) The life test of ND-f, ND-1300 and ND-2000 at 900°C. d) The influence of surface O% by XPS (right to-left corresponding to ND-f to ND-2000) and BET surface area (top to-bottom corresponding to ND-f to ND-2000) on initial reaction rate. Conditions: 150 mg sample, 10% $CH_4$, balanced in $N_2$, total flow rate 50 mL $min^{-1}$, GHSV=20000 $h^{-1}$.

To rule out the effect of oxygen functional groups, we annealed the ND-f sample inside the reactor at 900°C for 1 hour to eliminate almost all oxygen atoms, and then conducted the reaction in situ. As shown in Fig. S3, there was less than 6% of drop at the beginning of reaction, and, after 5 h, the reaction rate was almost same with the untreated ND-f. We therefore conclude that surface oxygen atoms can only enhance the initial activity to some extent instead of playing a pivotal role. Along with the CMD process, the deposited carbon always causes the loss of activity.[7a] Fig. S4 shows that both BET surface area and pore volume of ND-f decreased with the time on steam, confirming the carbon-deposited mechanism for catalyst deactivation. Thermal treatment at 1300°C can improve the porosity and benefit the catalyst tolerating a great amount of carbon deposits before the catalyst deactivates.

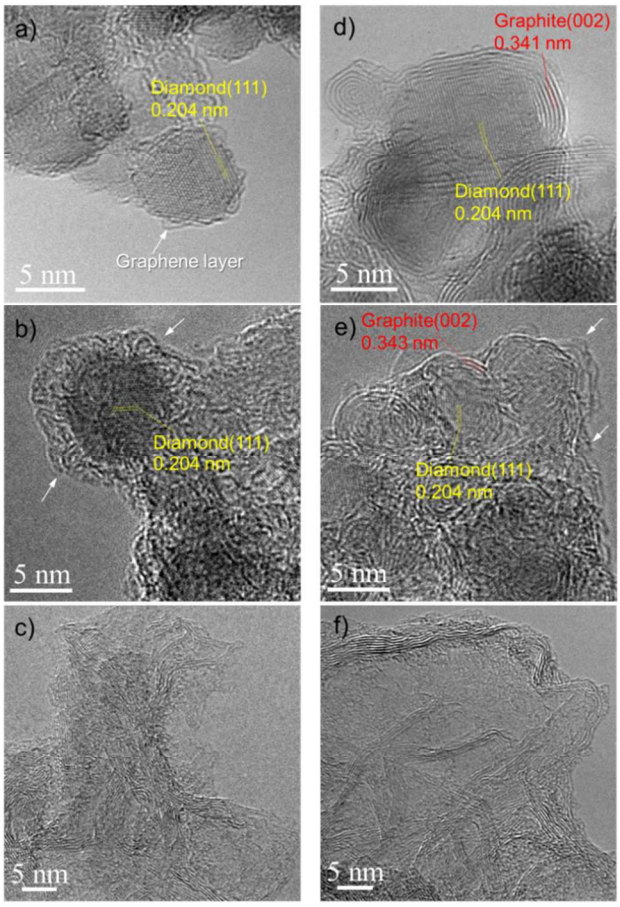


**Fig. 2** Transmission electron microscopy images of ND-f and ND-1300; a-c) ND-f at 0, 1, 20 h on stream, and, d-f) ND-1300 at 0, 1, 20 h on stream.

The morphology of the ND samples was investigated by the high resolution TEM as shown in Fig. 2. The lattice spacing distance of 2.04 Å and 3.35 Å were assigned to the (111) plane of diamond and (002) plane of graphite, respectively. It is indicated that the ND-f particles are constructed by diamond as cores and defective graphene as shells (Fig. 2a). For the ND-f, the by-product carbon immediately deposited to form a petaloid structure during the first hour on the stream (Fig. 2b). The reaction for 20 hours brought about few-layered graphene with a turbostratic structure (Fig. 2c), during which the graphitization of deposited carbon at the reaction temperature cannot be neglected. Annealing at 1300°C induced the graphitization of $sp^3$-hybridized carbon atoms to generate few-layered graphene sheets on the surface of ND-1300 (Fig. 2d). The amount of deposited

carbon was low at the beginning of reaction due to the inferior initial activity (Fig. 2e). Different with the ND-f sample, few-layered graphene sheets with a bigger size and enhanced ordering were found on ND-1300 after 20 hours on stream (Fig. 2f). To sum up, the annealed ND samples displayed an inferior activity at the beginning of reaction but such a slow process may allow the carbon species assembling into a much ordered structure like large-area few-layered graphene.

To elucidate the reaction mechanism over ND catalyst and the structure of catalytically active sites, we thoroughly investigated the fresh and used catalysts by surface science methods. Because surface oxygen groups were already ruled out (Fig. S3), the oxygen-free structural defects in graphene matrix were possible active sites to trigger the catalytic process. X-ray photoelectron spectroscopy (XPS) and static secondary ion mass spectroscopy (SIMS) are used to characterize the surface defects of carbon materials.[11] The peak width at half height of C*1s* spectra is related to indicate the presence of several defective structures like vacancy and topological defects.[12] Table S2 summarized the binding energies, FWHM of C*1s* spectra and $sp^2/sp^3$ ratio of the ND catalysts. The C1s spectra revealed the coexistence of $sp^3$ diamond and $sp^2$ graphite phases, as confirmed by the peaks at 286.7 and 284.5 eV, respectively.[8] Thermal annealing treatment of the ND-f sample gave rise to the $sp^2/sp^3$ ratio but decreased the FWHM value. Especially, a fairly good linear relationship was found between initial reaction rate and C*1s* FWHM value (Fig. 3a), suggesting that surface defects are most possibly essential for the catalytic activity.

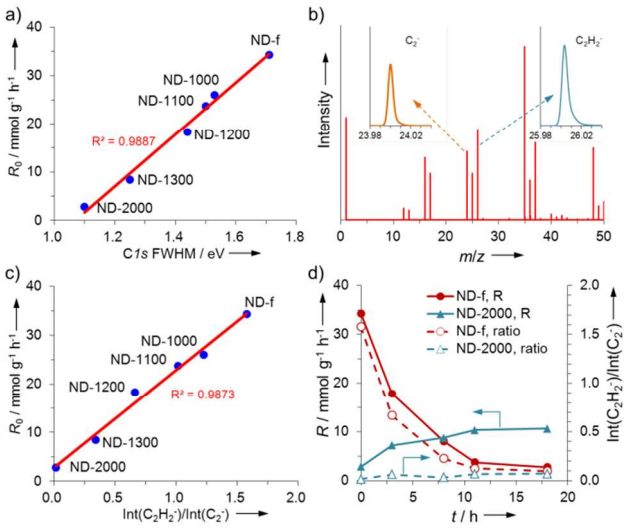


**Fig. 3** a) Relationship between initial reaction rate and FWHM of the XPS graphite peak at 284.5eV. b) SIMS spectrum of ND-f. c) Relationship between initial reaction rate and $C_2H_2^-/C_2^-$ of NDs. d) Profiles of reaction rate and $C_2H_2^-/C_2^-$ ratio of ND-f and ND-2000 along with the time on stream.

SIMS is capable to detect the first atomic layers of carbon materials, as well to profile all ejected fragments from the surface during the bombardment of high-energy ions. The SIMS spectrum of ND-f in Fig. 2b shows intense peaks of negatively charged $C_2H^-$, $C_2H_2^-$ and $C_2^-$ fragment ions. The $C_2H^-$ and $C_2^-$ signals are regarded as good measures for the amounts of aromatic C-H groups and aromatic/graphitic carbon,[13] respectively. The ratio of the $C_2H^-/C_2^-$ peak is therefore reported as a direct measure of the surface concentration of aromatic C-H groups.[13] In positive SIMS spectra, the signal of $CH_y^+$ (y=1-3) indicates the presence of aliphatic C-H groups on the surface.[13a] The signal of $C_2H_2^-$ as an acetylene-like fragment normally increased with the surface erosion time, which is seen as the a helpful fingerprint indicating the hydrogenated defects embedded inside the graphitic matrix rather than the poorly crystalline species.[14] The attempts to correlate the initial activity with the intensity of fragments, except for $C_2H_2^-$, have failed to give a monotonic tendency (Fig. S5). As shown in Fig. 3c, the initial reaction rate of CMD shows a linear relationship with the $C_2H_2^-/C_2^-$ ratio of NDs that annealed at different temperatures. We therefore conclude that the decomposition of methane is most possibly governed by the defective sites that can release $C_2H_2^-$ fragments in SIMS spectra.

We characterized the ND catalysts that reacted for different times to follow the variation of active site with the time on stream. As seen in Fig. 3d, with the reaction approached, the $C_2H_2^-/C_2^-$ ratio of ND-f significantly decreased while that of ND-2000 slightly increased. Reaction rate and $C_2H_2^-/C_2^-$ ratio show a similar tendency with the increasing reaction time, confirming a determining role of the $C_2H_2^-/C_2^-$ ratio on the CMD process. In view of the negligible effect of oxygen groups and poorly crystalline species, we are inclined to recognize the unsaturated edges or vacancies in graphene sheet as the active sites.

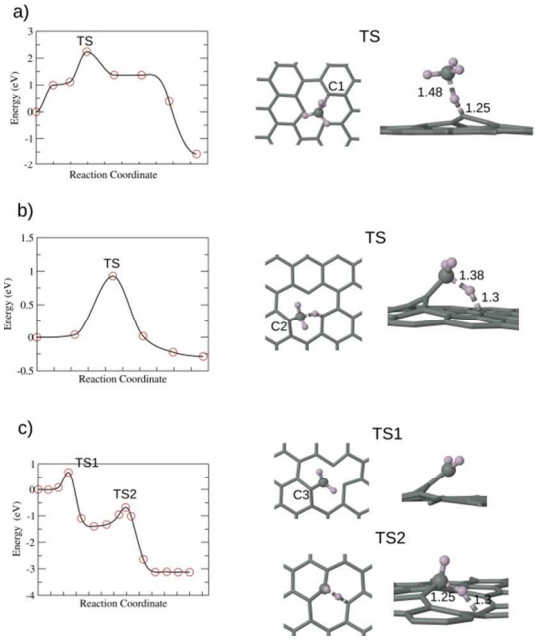


**Fig. 4** The minimum energy path and structures of the transition states for (a) $CH_4 \rightarrow CH_3+1/2H_2$, (b) $CH_3 \rightarrow CH_2+1/2H_2$, (c) $CH_2 \rightarrow C+H_2$.

First-principles density functional theory (DFT) calculations were performed to help understanding the reaction pathways and mechanism. The defective sites such as vacancies and edges on carbon catalysts are suggested as the active sites in the $CH_4$ decomposition.[15] In current calculations, a mono-vacancy on graphene is used to mimic the active site in the reaction as shown in Fig. 4. It is known that the $CH_4$ molecule has a large C–H bond

energy of 413 kJ/mol and the initial C-H bond cleavage has been discussed in literature as the rate-limiting step.[16] The calculated energy of this process is estimated to be 2.47 eV that is indeed the largest barrier obtained in the CMD reaction. As seen in Fig. 4a, at the transition state the $CH_4$ molecule interacts with one of the carbon atoms around vacancy and then one hydrogen atom breaks off from $CH_4$ forming a bond with the carbon around vacancy (C1), producing a $–CH_3$ group. The distances for the breaking and forming C–H bonds are 1.48 and 1.25 Å, respectively. The first C-H bond dissociation step is exothermic and the estimated value is 1.57 eV. The resulted $–CH_3$ group is possible to further lose the hydrogen at the vacancy site (Fig. 4b). The barrier is 0.93 eV and it is still an exothermic process by 0.29 eV. After the second C–H bond of $CH_4$ is broken, the $–CH_2$ group is populated around vacancy (C2). The minimum energy path (MEP) for further scission of C–H bond in $–CH_2$ group is depicted in Fig. 4c, which is obviously different and displays two transition states (TS). TS1 represents the approach to another carbon atom around vacancy (C3) while TS2 originates from the breaking of the C–H bond, overcoming two barriers of 0.68 and 0.64 eV, respectively. From the theoretical viewpoint, these kinds of vacancy sites are capable to inspire the dissociation of $CH_4$ and the newly generated defects may coordinate the growth of graphene layers over a long period of time.

## Conclusions

In summary, we have applied purified commercial nanodiamond as a novel catalyst for methane decomposition reaction. In addition to a superior activity and stability to the other carbon materials, we are delighted to observe the formation of well-graphitized few-layered graphene as the solid product. Both XPS and SIMS experiments confirmed that the catalytic activity is essentially dependent on the defective sites embedding inside the graphene matrix. The reaction rate was correlated for the first time with the $C_2H_2^-/C_2^-$ ratio and obeyed an excellently linear correlation. The possible mechanism was proposed as a series of surface stepwise dissociation reactions of $CH_x$ (x=1-4) to form layered graphene and molecular $H_2$.

## Acknowledgements

We gratefully acknowledge financial supports from the National Natural Science Foundation of China (projects 51202262, 50921004, 20973079, 21133010) and Ministry of Science and Technology of People's Republic of China (project 2011CBA00504).

## Notes and references

[a]*University of Science and Technology of China, 96 Jinzhai Road, Hefei, 230026, China*
[b]*Catalytic Materials Division, Shenyang National Laboratory for Materials Science, Institute of Metal Research, Chinese Academy of Sciences 72 Wenhua Road, Shenyang 110016, China. E-mail: dssu@imr.ac.cn*
[c]*Ningbo Institute of Materials Technology & Engineering, Chinese Academy of Sciences 519 Zhuangshi Road, Ningbo 315201, China. E-mail: jzhang@nimte.ac.cn*

† Electronic Supplementary Information (ESI) available: Detail experimental and the characterization of the samples. See DOI: 10.1039/b000000x/

1 R. Guil-Lopez, J.A. Botas, J.L.G. Fierro and D.P. Serrano, *Applied Catalysis A: General*, 2011, **396**, 40.
2 S. Hofmann, G. Csányi, A.C. Ferrari, M.C. Payne and J. Robertson, *Phys. Rev. Lett.,* 2005, **95**, 036101.
3 N.Q. Zhao, C.N. He, J. Ding, T.C. Zou, Z.J. Qiao, C.S. Shi, X.W. Du, J.J. Li and Y.D. Li, *J. Alloys. Compd.*,2007, **428,** 79.
4 N. Muradov, F. Smith and A. T-Raissi, *Catal. Today*, 2005, **102**, 225.
5 D. S. Su, J. Zhang, B. Frank, A. Thomas, X. Wang, J. Paraknowitsch and R. Schlögl, *ChemSusChem,* 2010, **3**, 169.
6 a) J. Zhang, X. Liu, R. Blume, A. Zhang, R. Schlögl and D. S. Su, *Science,* 2008, **322**, 73; b) K. Gong, F. Du, Z. Xia, M. Durstock and L. Dai, *Science,* 2009, **323**, 760; c) B. Frank, A. Rinaldi, A. Trunschke and R. Schlögl, *Angew. Chem. Int. Ed.*, 2011, **50**, 1.
7 a) R. Moliner, I. Suelves, M.J. Lázaro and O. Moreno, *Int. J. Hydrogen Energy*, 2005, **30**, 293; b) E. K. Lee, E.K. Leea, S.Y. Lee, G.Y. Han, B.K. Lee, T.-J. Lee, J.H. Jun and K.J. Yoon, *Carbon*, 2004, **42**, 2641; c) A. Dufour, A. Celzard, V. Fierro, E. Martin, F. Broust and A. Zoulalian, *Appl. Catal. A: Gen.*, 2008, **346**, 164.
8 a) J. Zhang, D.S. Su, R. Blume, R. Schlögl, R. Wang, X. Yang and A. Gajović, *Angew. Chem. Int. Ed.*, 2010, **49**, 8640; b) S. Osswald, G. Yushin, V. Mochalin, S.O. Kucheyev and Y. Gogotsi, *J. Am. Chem. Soc.*, 2006, **128**, 11635.
9 a) G.P. Bogatyreva, M.A. Marinich, E.V. Ishchenko, V.L. Gvyazdovskaya, G.A. Bazalii and N.A. Oleinik, *Phys. Solid State*, 2004, **46**, 738; b) L.H. Chen, J.B. Zang, Y.H. Wang and L.Y. Bian, *Electrochem. Acta*, 2008, **53**, 3442.
10 J. Zhang, D.S. Su, A. Zhang, D. Wang, R. Schlögl and C. Hébert, *Angew. Chem. Int. Ed.*, 2007, **46**, 7319.
11 a) P. Albers, B. Freund, G. Prescher, K. Seibold and S. Wolff, *Kautsch. Gummi Kunstst.,* 1995, **48**, 336; b) P. Albers, K. Deller, B.M. Depeyroux, A. Schäfer and K. Seibold, *J. Catal.*, 1992, **133**, 467; c) J.A. Ayala, W.M. Hess, F.D. Kistler and G.A. Joyce, *Rubber Chem. Technol.*, 1991, **64**, 19.
12 D.P. Serrano, J.A. Botas, J.L.G. Fierro, R. Guil-López, P. Pizarro and G. Gómez, *Fuel*, 2010, **89**, 1241.
13 a) D. Hans, C. Abdelkader, R. Christian and K. Serge, *Fuel*, 1996, **75**, 125; b) D. Hans, S. Lydia, R. Ulf, R. Christian, K. Serge and A. Alain, *Surf. Interf. Anal.*, 1997, **25**, 245; c) O.L. Eryilmaz and A. Erdemir, *Wear*, 2008, **265**, 244.
14 W.A. Peter, K. Harald, S.L. Egbert, S. Klaus, P. Günter and F.P. Stewart, *Phys. Chem. Chem. Phys.*, 2000, **2**, 1051.
15 a) L.M. Aparicio, *J. Catal.*, 1997, **165**, 262; b) M.C.J. Bradford and M.A. Vannice, *Appl. Catal. A.*,1996, **142**, 97.
16 a) B. Li and H. Metiu, *J. Phys. Chem. C*, 2011, **115**, 18239; b) W. Tang, Z.P. Hu, M.J. Wang, G.D. Stucky, H. Metiu and E.W. McFarland, *J. Catal.*, 2010, **273**, 125.



 